Letter

Atomic-Level Design of Water-Resistant Hybrid Perovskites for Solar Cells by Using Cluster Ions

Hong Fang, and Puru Jena

J. Phys. Chem. Lett., **Just Accepted Manuscript** • DOI: 10.1021/acs.jpclett.7b01529 • Publication Date (Web): 27 Jul 2017

Atomic-Level Design of Water-Resistant Hybrid Perovskites for Solar Cells by Using Cluster Ions

Hong Fang and Puru Jena*

Department of Physics, Virginia Commonwealth University, 701 West Grace Street, VA, 23284, United States. *Email: pjena@vcu.edu

Abstract

Organic-inorganic hybrid perovskites have emerged as the most promising material in the development of next-generation solar cells. However, the stability of these materials exemplified by $CH_3NH_3PbI_3$ is the most pressing challenge; it readily decomposes when exposed to moisture. Here, we show how one can use a particular type of cluster ions, known as pseudohalides, to enhance the water resistance of the hybrid perovskite, while maintaining its favorable electronic properties. Starting with a simple physical model, we propose a new class of water-resistant hybrid perovskites as solar-cell absorbers based on the cluster ions by using DFT calculations and *ab initio* molecular dynamics. Limitations of applying the currently known pseudohalides for our purpose are also discussed.

TOC Image

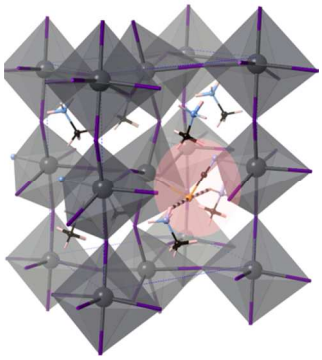

Organic-inorganic hybrid perovskites, exemplified by $MAPbI_3$ (MA = CH_3NH_3, methylammonium), have become the super-star absorber materials for solar cells. They are easy to make from solution or vapor and their power conversion efficiency (PCE) exceeded 20% within only five years.[1-11] However, due to its intrinsic instability towards moisture,[12-15] $MAPbI_3$ readily decomposes with a trace amount of water and quickly loses the initial PCE, which is the most pressing challenge in the field. Besides the use of protective layers or encapsulating techniques,[16,17] the counter measure to make the hybrid perovskite water-resistant is to enhance its stability by adjusting its compositions. Indeed, greater stability can be achieved by mixing cations MA, FA (formamidinium) and Cs as well as halogens I and Br.[17,18] Alternatively, by partially replacing I with thiocyanate (SCN^-), the resulting $MAPbI_{3-x}(SCN)_x$ shows greatly improved stability against moisture while retaining about 80% of the original PCE.[19] Here, by introducing cluster ions into the composition of the hybrid perovskite, we follow an atomic-level design approach to enhance its stability against moisture, while controlling its electronic properties at the same time. Based on this, we propose a new set of moisture-resistant hybrid perovskites. We also discuss limitations of using the cluster ions to improve the stability and the PCE of the hybrid perovskite.

In our previous study of hybrid perovskites AMX_3,[15,20,21] we introduced a new paradigm for these materials by showing that it is possible to view them as "super" alkali halides. Here, the organic cations A^+ (A = MA, FA) can be viewed as super-alkali ions whose ionization potentials are lower than that of lithium.[22] Similarly, the inorganic anions $[MX_3]^-$ (M = Pb, Sn, Ge; X = halogen) can be viewed as super-halogen ions whose electron affinities are higher than that of chlorine.[23] We showed that, as in the

alkali halides, the bandgaps and the band alignment of the hybrid perovskites are largely determined by the ionic radii of the super-alkali cation (A^+) and the super-halogen anion ($[MX_3]^-$), as well as the bonding ionicity between them.[15] In fact, the bulk electronic properties of these "super" alkali halides resemble the electronic properties of the corresponding molecular clusters $A[MX_3]$,[20] as shown in Fig. 1a. We also showed that the degradation of $MAPbI_3$ in the presence of a trace amount of water could be understood by focusing on the interaction of the representative molecular cluster with water. As shown in Fig.1b, a water molecule is found to be trapped between the organic cation MA^+ and the inorganic anion $[PbI_3]^-$ due to the Coulomb attraction. Molecular dynamics (MD) simulations carried out on the molecular building block further showed that the degradation mechanism involves H_2O serving as a "catalyst" to remove I^- from $[PbI_3]^-$ which in turn combines with H^+ of the organic cation, resulting in the formation of HI and PbI_2.[15]

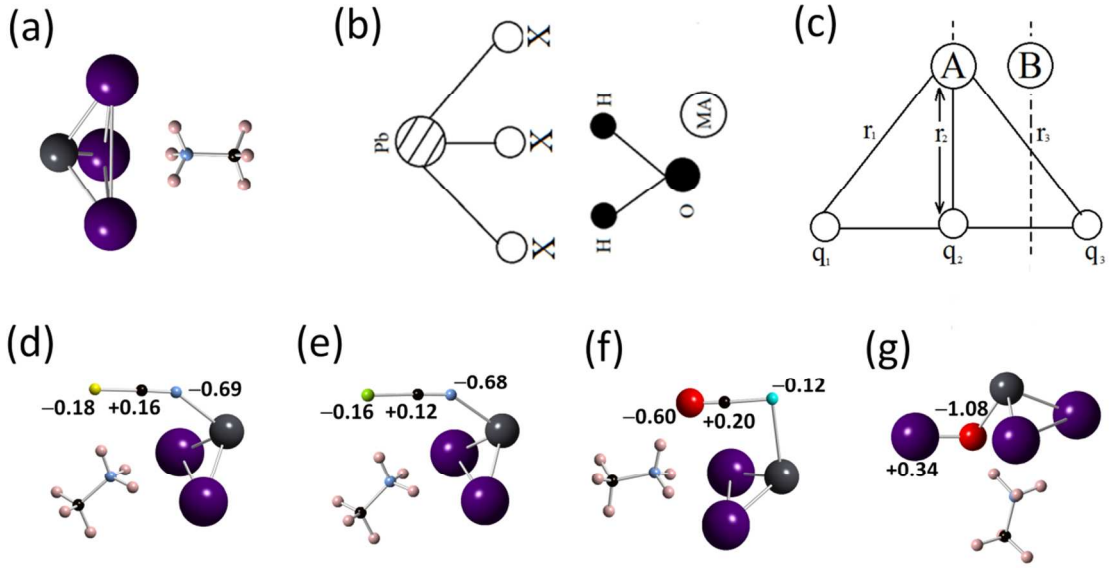

Fig. 1 (a) Optimized molecular cluster of $MAPbI_3$. (b) The physical model of a water molecule trapped inside the $MAPbX_3$cluster where the two positive hydrogen atoms in the water molecule are attracted to the negative halogen X of $[PbX_3]^-$while the negative oxygen of the water molecule is attracted to the positive hydrogen atoms in the organic cation MA^+ ($CH_3NH_3^+$). (c) The schematic demonstration of a water molecule approaching the cluster ion with an internal charge distribution of q_1, q_2 and q_3 on the three constituent atoms. (d)-(g) The optimized cluster models of $MAPbI_2$(SCN), $MAPbI_2$(SeCN), $MAPbI_2$(PCO)and $MAPbI_2$(OI), respectively. The corresponding clusters of $MAPbI_2$(OCl) and $MAPbI_2$(OBr) are shown in Fig. S3 of SI. The numbers in each case show the internal charge distribution of the cluster ion using the NBO analysis (see Method). The color scheme is: Pb in dark grey, I in purple, C in black, N in light blue, H in pink, S in yellow, Se in orange, O in red and P in cyan.

The strategy to address the degradation process is twofold: First, reduce the interaction between the water molecule and $[PbX_3]^-$ so that the water molecule is unlikely to be trapped between the cation and the anion. Second, enhance the bonding between Pb and X in $[PbX_3]^-$ so that X^- is unlikely to be dislodged from the group. We will show that one can achieve both of the above by replacing halogens X by cluster ions. Reduction of the Coulomb interaction between a negative cluster ion and the water molecule approaching it from distance is a constrained optimization problem: how to distribute a

total charge of $Q = -1$ on the cluster ion such that the Coulomb interaction minimized. Given a cluster ion with a linear (rod-like) configuration (e.g. SCN^-) as shown in Fig.1b, one needs to find the minimum of the following function,

$$F = \left(\frac{q_1}{r_1} + \frac{q_2}{r_2} + \frac{q_3}{r_3} \right)^2 + \lambda \left(q_1 + q_2 + q_3 - Q \right), \quad (1)$$

where q_1, q_2 and q_3 are the atomic charges on the three constituent atoms of the cluster ion. $Q = -1$ is the total charge of the cluster ion. r_1, r_2 and r_3 are the distances between the water molecule and the atoms carrying charges q_1, q_2 and q_3, respectively. λ is the Lagrange multiplier. The problem is to find a situation when the Coulomb potential has the minimum magnitude by solving,

$$\frac{\partial F}{\partial \lambda} = 0; \quad \frac{\partial F}{\partial q_1} = 0; \quad \frac{\partial F}{\partial q_2} = 0 \quad \frac{\partial F}{\partial q_3} = 0 . \quad (2)$$

In the Supporting Information (SI), we give the relevant special solutions to the problem. We find that, if a water molecule approaches the cluster ion along the middle line as shown in Fig.1c by spot "A", it would be better to have the middle atom positively charged and the atoms at the two ends negatively charged. If a water molecule approaches the cluster ion closer to one of its end as shown in Fig.1c by spot "B", it would be better to have the atom at the far end (relative to the water molecule at "B") to assume most of the negative charge, while the other two atoms assume small charges with opposite signs.

Table 1. The ionic radii (R), vertical detachment energy (VDE), internal charge distribution and the vibrational frequency (IR) of Pb-X (X = I, S-C-N, P-C-O, O-Cl, O-Br and O-I) bonding of the proposed cluster ions. The ionic radius of a cluster ion is calculated by using its bond length and 0.30 Å for the ionic radius of carbon. We found that the calculated ionic radii are same in the optimized cluster models and the crystals. See the Method section for the analysis of internal charge distributions.

Ion	R (Å)	VDE (eV)	NBO (Bader)					IR (cm^{-1})
I^-	2.1	3.30	Pb +0.17 (+0.92)			I –0.51 (–0.54)		128.8
SCN^-	2.5	3.52	Pb +0.96 (+0.98)	I –0.52 (–0.56)	S –0.18 (–0.00)	C +0.16 (+0.55)	N –0.69 (–1.25)	231.1
$SeCN^-$	2.7	3.39	Pb +0.96 (+0.95)	I –0.51 (–0.55)	Se –0.16 (–0.02)	C +0.12 (+0.64)	N –0.68 (–1.25)	202.4
PCO^-	2.5	2.74	Pb +0.72 (+0.92)	I –0.51 (–0.54)	O –0.60 (–1.10)	C +0.20 (+0.26)	P –0.12 (+0.25)	197.4
ClO^-	1.7	2.32	Pb +0.97 (+0.96)	I –0.52 (–0.54)	O –0.88 (–0.81)	Cl +0.14 (+0.07)		345.9
BrO^-	1.9	2.40	Pb +0.98 (+0.95)	I –0.54 (–0.53)	O –0.96 (–0.93)	Br +0.21 (+0.12)		339.2
IO^-	2.0	2.46	Pb +0.98 (+0.94)	I –0.54 (–0.54)	O –1.08 (–1.06)	I(O) +0.34 (+0.30)		334.5

Meanwhile, it is important to understand the implication on the electronic structure of the hybrid perovskites when using cluster ions to replace iodine in $MAPbI_3$. As discussed at the beginning, we have found that the bandgap of $MAPbX_3$ depends on the size of the super-halogen ion $[PbX_3]^-$ and its bonding ionicity with the super-alkali ion MA^+. The trend is that the larger the size of $[PbX_3]^-$ and the lower the bonding ionicity, the smaller is the bandgap of the material. With the MA^+ cation, the bonding ionicity merely depends on the ability of $[PbX_3]^-$ to hold the valence electron. Such ability can be

measured by the vertical detachment energy (VDE) of $[PbX_3]^-$ and, consequently, by the VDE of X^-.[15] Smaller VDE of X^- corresponds to weaker holding capability of the valence electron in $[PbX_3]^-$. This in turn suggests lower bonding ionicity and smaller bandgap of $MAPbX_3$. For example, the VDE of halogens decreases with increasing size from chlorine to iodine. Note that the bandgap of $MAPbX_3$ also decreases from X = Cl to I.

Based on this idea, if some cluster ion is to be used to replace iodine in $MAPbI_3$ to enhance its stability against moisture, the cluster ion should have a similar or smaller VDE than that of iodine so that such replacement will not compromise the desired bandgap of $MAPbI_3$. In Table 1, we list the known candidates for such cluster ions. Their optimized structures are shown in Fig. S1 of SI. All of them have similar or lower VDE than that of iodine and, therefore, are known as pseudohalides. Among these, thiocyanate SCN^- has the largest VDE.[24] Selenocyanate, $SeCN^-$, has a slightly smaller VDE than that of SCN^-. PCO^-, having much lower VDE compared to SCN^-, is formed by the same group elements (group 6, 4 and 5 in the periodic table) of SCN^-, OCl^-, OBr^- and OI^- are known as hypochlorite, hypobromite and hypoiodite ions, respectively. These ions have smaller VDE than that of SCN^-. All the pseudohalides have similar or smaller ionic radii than those of I^- and SCN^-. Since the stability of the 3D perovskites is according to the Goldschmidt tolerance factor which is not sensitive to the ionic radius of the halogen, similar ionic radii of the pseudohalides compared with I^- and SCN^- suggests that these cluster ions can stabilize the 3D perovskite structure as seen experimentally for the $MAPbI_{2.75}(SCN)_{0.25}$.[19]

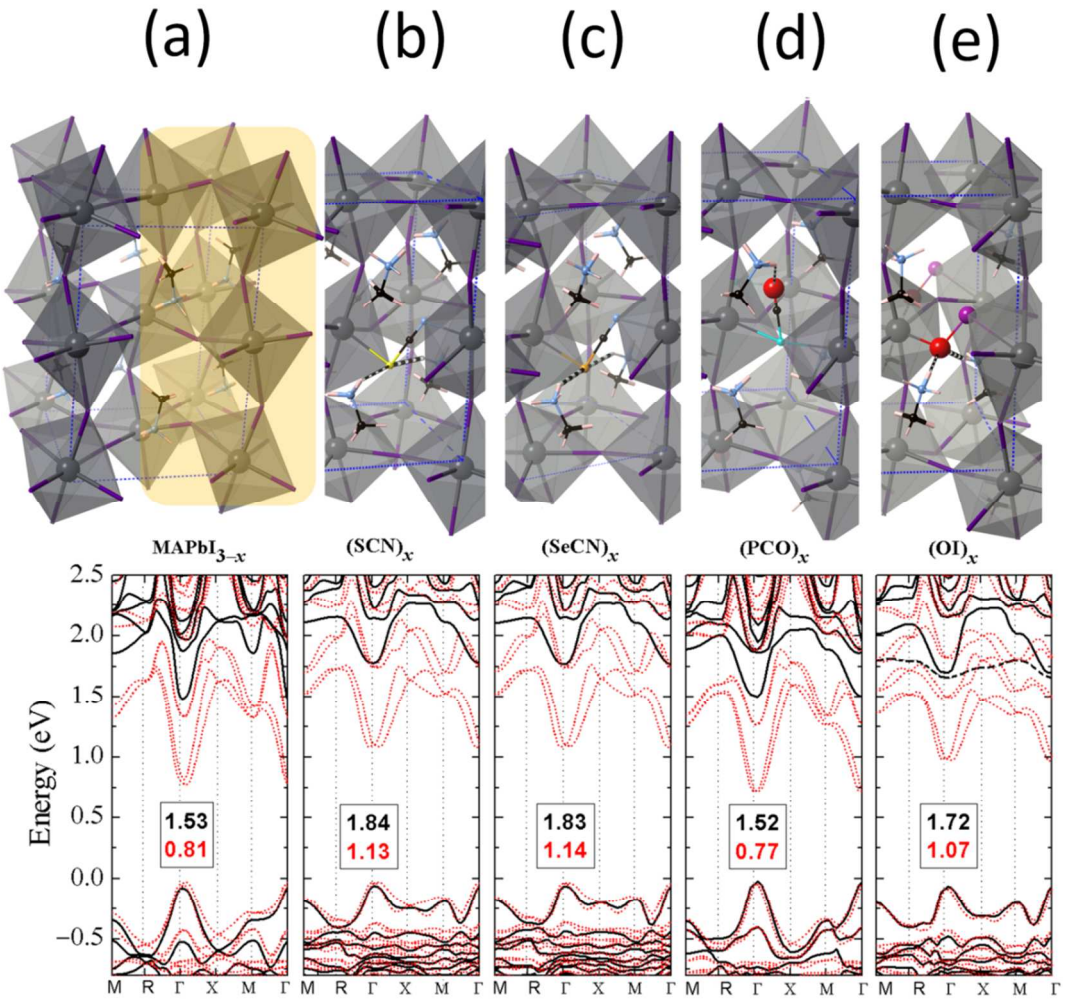

Fig. 2 Optimized unit cells of the crystals (a) $MAPbI_3$ and (b)-(e) $MAPbI_{2.75}(ph)_{0.25}$ (ph = SCN, SeCN, PCO and OI), together with their calculated band structures with (in red) and without (in black) the spin-orbit coupling (SOC). The corresponding results of $MAPbI_{2.75}(OCl)_{0.25}$ and $MAPbI_{2.75}(OBr)_{0.25}$ are given in Fig. S2 of SI. In each case, the number in black is the bandgap without SOC and the number in red is the bandgap with SOC. All the materials show direct bandgap at the Γ point. For $MAPbI_{2.75}(OI)_{0.25}$, the conduction band without inclusion of SOC (indicated by the black dashed line) is from the halogen. With SOC, the conduction band arised from Pb. The color scheme is: Pb in dark grey, I in purple, C in black, N in light blue, H in pink, S in yellow, Se in orange, O in red and P in cyan. Refer to Method for additional details.

As experimentally reported, only a "dilute" replacement of I^- by SCN^- in $MAPbI_3$ is needed to enhance the stability of $MAPbI_{2.75}(SCN)_{0.25}$ against moisture.[19] In fact, the "dilute" replacement is preferred so that the original electronic structure, and hence, the original PCE of the material could be retained. Thus, we study the electronic structures of

the pseudohalogen substituted hybrid perovskites in the "dilute" limit. Similar to the reported $MAPbI_{2.75}(SCN)_{0.25}$,[19] we obtain a series of hybrid perovskites $MAPbI_{2.75}(ph)_{0.25}$ with "dilute" replacement of I by the pseudohalogens ph = SeCN, PCO, OCl, OBr and OI based on the crystal structure of $MAPbI_3$ (see Method). These are shown in Fig. 2 and Fig. S2 of SI. To measure the intrinsic stability of the pseudohalide perovskites, we study the energy needed to replace one I^- by a pesudohalide "ph^-" in the unit cell of $MAPbI_3$,

$$\Delta E^{\mathrm{ph}} = E_{\mathrm{p}} - E_{\mathrm{r}}, \quad (3)$$

where E_{p} and E_{r} are the energies of the two sides of the reaction,

$$\underbrace{4 \cdot MAPbI_3 + ph^-}_{E_{\mathrm{r}}} \rightarrow \underbrace{4 \cdot MAPbI_{2.75}ph_{0.25} + I^-}_{E_{\mathrm{p}}}. \quad (4)$$

A smaller (more negative) ΔE^{ph} means that the pseudohalide perovskite $MAPbI_{2.75}(ph)_{0.25}$ is more stable. Since, for ph = SCN, $MAPbI_{2.75}(SCN)_{0.25}$ has already been successfully synthesized,[19] we will use the ΔE^{SCN} as a benchmark value and calculate

$$\Delta E = \Delta E^{\mathrm{ph}} - \Delta E^{\mathrm{SCN}} \quad (5)$$

for the other pseudohalogens. As shown in Table 2, for $MAPbI_{2.75}(ph)_{0.25}$ with ph = SeCN, PCO, OCl, OBr and OI, their ΔE are all negative, suggesting that the intrinsic stability of these materials is higher compared to $MAPbI_{2.75}(SCN)_{0.25}$.

Table 2 Calculated ΔE (eV) as defined in Eqs (3)-(5) for the pseudohalide perovskites.

$MAPbI_{2.75}(ph)_{0.25}$, ph =	SCN	SeCN	PCO	OCl	OBr	OI
ΔE	0	−0.54	−0.30	−1.06	−1.34	−1.38

The band structures of $MAPbI_{2.75}(ph)_{0.25}$ are given in Fig.2b-e and Fig. S2 of SI. The calculated bandgap of $MAPbI_{2.75}(SCN)_{0.25}$ is only slightly larger than that of $MAPbI_3$ and is in agreement with that reported earlier.[19] As shown in Table 3, $MAPbI_{2.75}(SCN)_{0.25}$ has slightly larger effective masses of carriers than those of $MAPbI_3$. The relatively large bandgap and effective mass of the carriers in $MAPbI_{2.75}(SCN)_{0.25}$ can partially explain its lower PCE compared to that of $MAPbI_3$. $MAPbI_{2.75}(SeCN)_{0.25}$ shows very similar electronic structure as that of $MAPbI_{2.75}(SCN)_{0.25}$. Among the series studied, $MAPbI_{2.75}(PCO)_{0.25}$ shows the smallest bandgap -- even smaller than that of $MAPbI_3$. Moreover, as shown in Table 3, the material has even smaller effective masses of the carriers than those of $MAPbI_3$. These suggest that $MAPbI_{2.75}(PCO)_{0.25}$ has the potential to exhibit similar or even better PCE than that of $MAPbI_3$. Compared to $MAPbI_{2.75}(SCN)_{0.25}$, all $MAPbI_{2.75}(Oh)_{0.25}$ (h = Cl, Br, I) show smaller bandgaps and similar effective masses of the carriers, suggesting that these new materials may achieve high PCE.

Table 3 Calculated isotropic hole (m_h), electron (m_e) and reduced [$\mu = m_h m_e/(m_h + m_e)$] effective masses of the studied hybrid perovskites (see Method). All values are reported in units of electron mass.

	m_h	m_e	μ
$MAPbI_3$	0.150	0.116	0.065[a]
$MAPbI_{2.75}(SCN)_{0.25}$	0.218	0.106	0.071
$MAPbI_{2.75}(SeCN)_{0.25}$	0.237	0.113	0.076
$MAPbI_{2.75}(PCO)_{0.25}$	0.136	0.108	0.060
$MAPbI_{2.75}(OI)_{0.25}$	0.196	0.120	0.074

[a]The calculated (DFT+SOC) value in the literature is 0.060.[25] The experimental value is 0.104±0.003.[26]

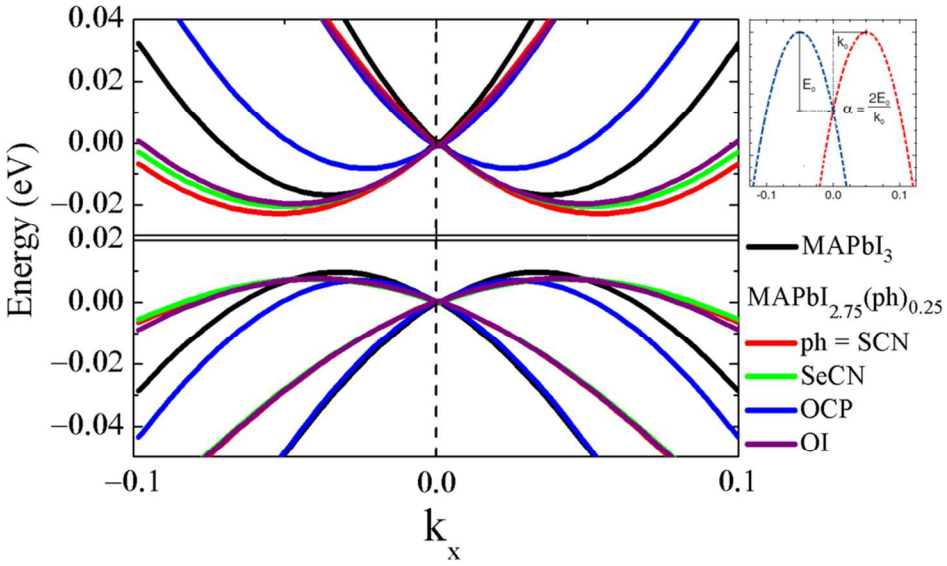

Fig. 3 Calculated Rashba splitting at the valence and conduction band edges of the hybrid perovskites composed of cluster ions. The schematic legend shows the definition of the Rashba parameter $\alpha = 2E_0/k_0$.

Besides the optimal bandgap and the decent mobility of the photo-excited carriers, the carriers' exceptionally long lifetime is the key to enable the high PCE of $MAPbI_3$. It has been found that the Rashba splitting on the band edges of the hybrid perovskite can significantly reduce the recombination rate and result in prolonged lifetime of the carriers.[27,28] The Rashba splitting is caused by the spin-orbit coupling (SOC) arising from the heavy Pb and the internal electric field created by the orientations of MA cations as well as the distortion of the Pb-I substructure. To study the influence of the cluster ions on the PCE of the hybrid perovskite, we calculated the Rashba splitting of the studied materials based on the tetragonal structure with I4*cm* space group. This has nonzero polarization caused by the tilted alignment of MA cations along the *c* axis. For simplicity, we assume that the dilute presence of the cluster ion will not modify the dynamical behavior of the material too much. Thus, to make a comparison with $MAPbI_3$, we only

consider the Rashba splitting with fixed orientation of MA and fixed positions of Pb and I atoms. The energy mismatch of the spin states and the mismatch of the momenta are given in Table 4. The calculated Rashba parameters in the table are about an order of magnitude smaller than those from a dynamical system, which is consistent with the finding in Ref. 29. All the hybrid perovskites with cluster ions show significant amount of Rashba splitting on the band edges, which reduces the recombination rate. Compared to $MAPbI_3$, the Rashba splitting energy of the hybrid perovskites with cluster ions are slightly smaller around the VBM. Around the CBM, the Rashba splitting energies of $MAPbI_{2.75}(SCN)_{0.25}$, $MAPbI_{2.75}(SeCN)_{0.25}$and $MAPbI_{2.75}(OI)_{0.25}$ are slightly larger than that of $MAPbI_3$. Generally speaking, the Rashba splittings of the hybrid perovskites with cluster ions are not much different from that of $MAPbI_3$. Since the amount of enhancement of the carrier lifetime depends on the magnitude of the Rashba splitting,[27] our results suggest that carriers in the hybrid perovskites with cluster ions would have a similar prolonged lifetime compared to that in $MAPbI_3$.

Table 4. The energy and momentum mismatch of the Rashba splitting as defined in Fig. 3. Rashba parameters of the studied materials are then calculated by $\alpha = 2E_0/k_0$. Values on the edges of the valence band (VB) and the conduction band (CB) are given for each case. $MAPbI_3$ shows the largest Rashba splitting among all.

Material	E_0 (eV)		k_0 (Å^{-1})		α (eV Å)	
	VB	CB	VB	CB	VB	CB
$MAPbI_3$	0.010	0.017	0.024	0.026	0.83	1.32
$MAPbI_{2.75}(SCN)_{0.25}$	0.008	0.023	0.029	0.037	0.56	1.27
$MAPbI_{2.75}(SeCN)_{0.25}$	0.008	0.020	0.028	0.035	0.55	1.14
$MAPbI_{2.75}(PCO)_{0.25}$	0.007	0.007	0.019	0.018	0.74	0.82
$MAPbI_{2.75}(OI)_{0.25}$	0.008	0.021	0.027	0.033	0.58	1.25

Now, we study the internal charge distribution of the pseudohalogen ions using both cluster models and the bulk crystals of the hybrid perovskites. The goal is to see if the charge distributions are consistent with the prediction of our electrostatic model introduced in Fig. 1c. As shown in Fig.1d-f, the internal charge distributions of SCN^-, $SeCN^-$ and PCO^- indeed satisfy the two requirements of the model. (1) The middle atom is positive and the atoms at the two ends are negative. (2) Most of the negative charge is concentrated on the atom at one end and the other two atoms bear smaller charges with opposite signs. Each of the cluster ions Oh^- (h = Cl, Br, I) can be seen as a special case of the cluster ion with three atoms, where two of the atoms are merged together. In such a case, the configuration of one positive atom at one end and one negative atom at the other, as shown in Fig. 1g and Fig. S3 of SI, generates weaker interaction with the water molecule than a single "–1" charge does. The internal charge distributions of these cluster ions inside the crystals are similar to those obtained in the cluster models, as shown in Table 1.

The use of charge distribution to reduce the electrostatic interaction between the cluster ions and the water molecule can be viewed as the physical side of the story, while the use of these cluster ions to strengthen the bonding inside $[PbX_3]^-$ can be viewed as the chemical side. From the calculated vibrational frequencies in Table 1, it is found that the bonding strength between Pb and the cluster ions are significantly stronger than that between Pb and I. The bonding strength of Pb-(PCO) is slightly weaker than those of Pb-(SCN) and Pb-(SeCN), while the bonding of Pb-$(Oh)_{h=Cl,Br,I}$ is much stronger.

All of the above discussions on the charge distribution and the bonding strength indicate that the pseudohalides should be able to significantly improve water resistance of the hybrid perovskites. We first test this by studying the water-cluster complexes with $MAPbI_2Y$ having "dilute" replacement of I by Y = pseudohalogens. For hO^- (h = Cl, Br, I) ions, since they show very similar internal charge distributions and bonding strength with Pb, we take BrO^- as the example. As shown by Fig. 4, in each case, the starting reactant is the water molecule trapped between MA^+ and $[PbX_3]^-$ optimized to the ground state. The optimized structures of $MAPbI_2(SCN)•H_2O$ and $MAPbI_2(SeCN)•H_2O$ are given in Fig. S4 of SI. The configuration of these ground states is consistent with our physical model in Fig. 1b. Since the internal charge distribution and the bonding strength of $MAPbI_2(SeCN)$ is very similar to those of $MAPbI_2(SCN)$ as shown in Table 1, good water-resistant ability is anticipated for $MAPbI_2(SeCN)$ (as already known for $MAPbI_2(SCN)$). According to MD simulations at 500K (see Method), the product state of $MAPbI_3•H_2O$ shows the separation of one I^- from $[PbI_3]^-$ and the separation of one H^+ from MA^+ ($[CH_3NH_3]^+$) to form HI and CH_3NH_2. On the other hand, the product states of $MAPbI_2(PCO)•H_2O$ and $MAPbI_2(BrO)•H_2O$ show complete detachment of the water molecule with intact $MAPbI_2(PCO)$ and $MAPbI_2(BrO)$, which clearly suggests the enhanced water resistance of the materials at the atomic level.

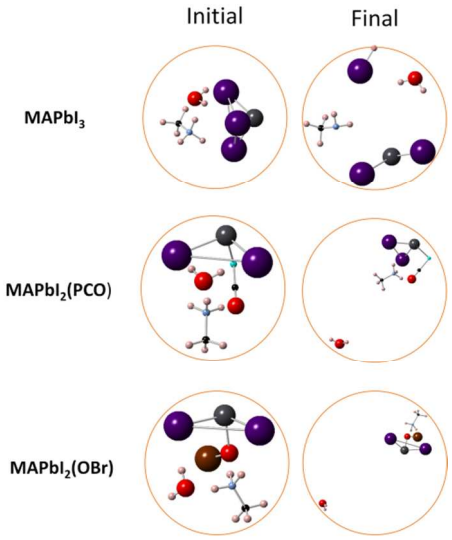

Fig. 4 Optimized ground states of cluster-water complexes of $MAPbI_3 \cdot H_2O$, $MAPbI_2(PCO) \cdot H_2O$ and $MAPbI_2(BrO) \cdot H_2O$ (initial). The ground states of $MAPbI_2(SCN) \cdot H_2O$ and $MAPbI_2(SeCN) \cdot H_2O$ are shown in Fig. S4. MD simulations at 500 K shows a complete detachment of the water molecule from intact clusters of pseudohalide perovskites (Final). This is compared with the disintegration of $MAPbI_3$ due to its reaction with water (Final). The color scheme is: Pb in dark grey, I in purple, C in black, N in light blue, H in pink, P in cyan, Br in brown and O in red.

We further test the stability of the materials in the bulk by conducting MD simulations with one water molecule inserted between MA^+ and $[PbX_3]^-$ in the bulk crystal. The optimized initial structures are given in Fig.S5 of SI. The stability of each structure is characterized by the calculated pair correlation functions (PCF), using the atomic trajectory data collected over 100 ps. As shown in the first two columns of Fig. 5, in each case, the PCF of Pb-X (X = I or pseudohalogens) is computed to evaluate their strength. The PCF of N-N, which is a measurement of distance between the organic cations in the crystal, is calculated to evaluate the lattice stability of the material under attack by water. For $MAPbI_3$, compared to the peaks of the ideal crystal structure without water, a new small Pb-I peak appears at a longer distance (around 5 Å) than the Pb's

closest neighboring iodine. This indicates the effect of water in separating some I atoms from the PbI_6 tetrahedra. Eventually, the whole lattice collapses as indicated by the complete disappearance of the characteristic peaks in the PCF of N-N. For $MAPbI_{2.75}(SCN)_{0.25}$ and $MAPbI_{2.75}(SeCN)_{0.25}$, however, the Pb-SCN and Pb-SeCN bonds hold still, evidenced by the appearance of the original peaks (around 3 Å) with broadening due to thermal vibrations. The lattice still shows strong characteristic peak in the PCF of N-N. For the case of $MAPbI_{2.75}(PCO)_{0.25}$, besides the original peak of the Pb-PCO bond at 3 Å, there is a new small peak that appears around 4.5 Å, which suggests large elongation of the bond. This is consistent with the fact that the bond strength of Pb-PCO is the weakest among the series as shown in Table 1. The material still shows a characteristic peak in the PCF of N-N but at a much smaller distance, indicating a phase transition caused by water as shown in Fig. S6 of SI.

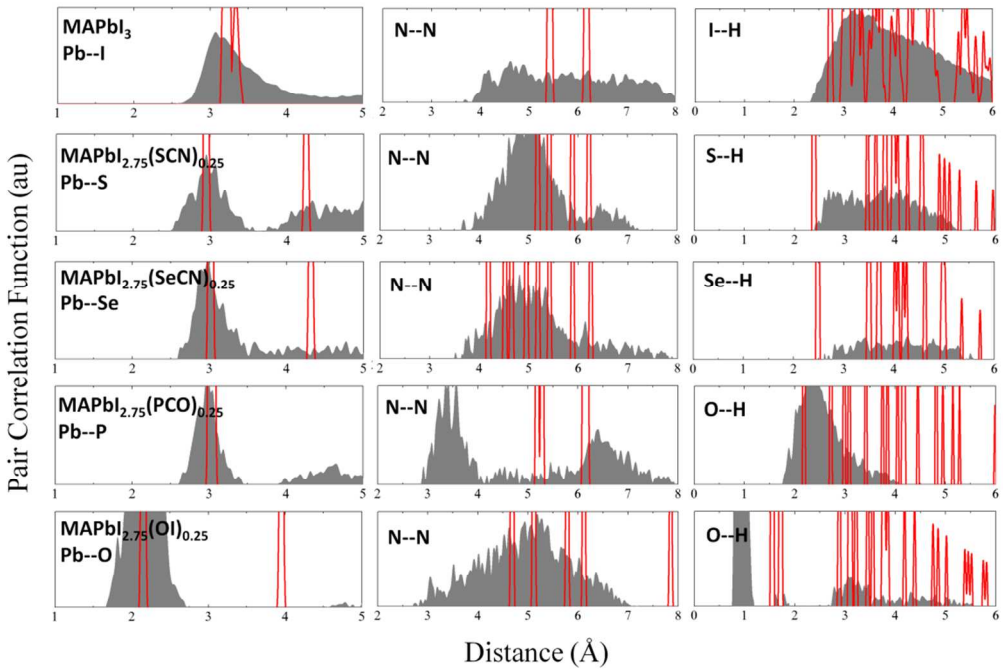

Fig. 5 The calculated pair correlation functions (PCF) of Pb-(pseudo)halogen, N-N and (pseudo)halogen-H from the atomic trajectory data of the MD simulations for materials $MAPbI_3•H_2O$, $MAPbI_{2.75}(SCN)_{0.25}•H_2O$,$MAPbI_{2.75}(SeCN)_{0.25}•H_2O$,$MAPbI_{2.75}(PCO)_{0.25}•H_2O$ and $MAPbI_{2.75}(OI)_{0.25}•H_2O$. In each column, the X and Y axes are put in the same scale. Refer to Method for additional details.

For $MAPbI_{2.75}(Oh)_{0.25}$ (h = Cl, Br, I), we choose $MAPbI_{2.75}(OI)_{0.25}$ as an example, since OI^- has the largest size in the series and hence make the largest space for water insertion to happen. As shown in the figure, the Pb-OI bond (around 2 Å) holds still and the lattice shows the strong characteristic peak in the PCF of N-N. However, as shown in the third column of Fig. 5, the peak in the PCF of O-H (with the hydrogen from MA) moves to less than 1Å after the simulated time for $MAPbI_{2.75}(OI)_{0.25}$, indicating that the OI^- seizes one hydrogen atom from the nearby MA^+ to form an O-H bond. This creates a defect of "CH_3NH_2 + O-H" in the crystal and is detrimental to the preferred electronic

structure. The process of forming the defect is shown in Fig. S6 of SI. Interestingly, the "CH_3NH_2 + O-H" defect in $MAPbI_{2.75}(OI)_{0.25}$, as shown by Fig. S7, can be completely removed after optimization at 0 K. This suggests that annealing may help to reduce such defect in $MAPbI_{2.75}(OI)_{0.25}$. For all the other studied materials as shown by the third column of Fig. 5, including $MAPbI_{2.75}(SCN)_{0.25}$, $MAPbI_{2.75}(SeCN)_{0.25}$ and $MAPbI_{2.75}(PCO)_{0.25}$, there is no sign of this defect formation, where one hydrogen atom from MA^+ is seized by the cluster ion.

Cluster ions with the proper internal charge distribution can enhance the water resistance of the hybrid perovskite by minimizing its interaction with water and strengthening the bond with Pb. To achieve the optimal bandgap with a value similar or slightly smaller than that of $MAPbI_3$, cluster ions called pseudohalides with VDEs similar or smaller than that of I^- are required. Besides the proper bandgap, pseudohalides can also retain the decent carrier mobility and the large Rashba splitting of $MAPbI_3$, which are essential to maintain the high PCE of the material. In line with these, a new class of water-resistant hybrid perovskites $MAPbI_{2.75}(ph)_{0.25}$ (ph = SCN, SeCN, PCO, OCl, OBr and OI) with preferred electronic properties are reported. The results can be readily generalized to make other water-resistant hybrid perovskites with different cations, such as FA^+ and Cs^+, different metal elements, such as Sn and Ge, as well as different halides, such as Br and Cl. Our study also shows limitations of the currently known pseudohalides. With the dilute replacement of iodine by the pseudohalides containing oxygen, the hybrid perovskite is likely to go through phase transition (in the case of $MAPbI_{2.75}(PCO)_{0.25}$) or form "CH_3NH_2 + O-H" defect (in the case of $MAPbI_{2.75}(OI)_{0.25}$) when exposed to water.

It is, therefore, highly desirable to develop new oxygen-free pseudohalides both theoretically and experimentally.

METHOD

Cluster calculations. The calculations are carried out using the GAUSSIAN03 package.[30] The hybrid density functional theory (DFT) with Becke three parameter Lee-Yang-Parr (B3LYP)[31,32] functional for the exchange-correlation energy and 6-31+G(d,p) basis sets are used. All the clusters are put in the neutral state with zero total spin. The optimized ground states correspond to the structures with the minimum energy and without any imaginary frequency.

Bulk calculations. Density Functional Theory (DFT) calculations are carried out to optimize the unit cell (based on the most stable tetragonal unit cell of $MAPbI_3$ with *I*4*cm* space group: $a=b=8.8490$Å; $c=12.6420$Å; $\alpha=\beta=\gamma=90.0000°$) of the studied hybrid perovskites. We used Perdew-Burke-Ernzerh (PBE) generalized gradient approximation (GGA) for exchange-correlation functional[33] implemented in the VASP package.[34] The projector augmented wave (PAW)[35] pseudopotential method and a $3\times3\times2$ Monkhorst-Pack k-point mesh are used in the calculation. The cutoff energy is 500 eV. The energy and the force convergence are set to 10^{-5} eV and 0.005 eV/Å, respectively. It is known that, for heavy metal element, spin-orbit coupling (SOC) is very important.[36] Therefore, the electronic structures of the materials are calculated with and without the SOC for comparison. The Rashba splitting at the band edges is calculated along the direction of (0, $-\xi$, 0) to (0, 0, 0) to (0, ξ, 0) in the k space. The van der Waals interaction (as implemented in the DFT + D2 method[37,38]) is considered during all the calculations.

Effective masses. The effective mass tensor

$$m_{ij}^{*} = \hbar \left(\frac{\partial^2 E}{\partial k_i \partial k_j} \right)^{-1} \quad \text{(m1)}$$

is calculated at the Γ point with respect to the wave vector **k** along the three crystallographic directions indexed by *i* and *j*. The second derivatives are numerically calculated with the finite difference method. Effective masses are obtained by diagonalizing the tensor. The isotropic hole and electron masses are the averaged eigenvalues of the valence and conduction band effective masses, respectively.

Internal charge distribution of the cluster ions. Natural Bond Orbital (NBO) analysis is used to calculate the internal charge distribution of the cluster ions in the cluster models. For crystals, Bader charge analysis is used to calculate distribution of electrons in the cluster ions.

Molecular dynamics simulations. Molecular dynamics (MD) simulations are conducted with normal precision in VASP using a tolerance of 1×10^{-5} eV for energy convergence in the SCF cycle. No symmetry constraint is imposed. Van der Waals dispersion interactions are considered using the DFT+D2 method. The time step is set to 1.0 fs. MD simulations (Fig. 4) are carried out at 500 K for the cluster models contained in a 25 Å × 25 Å ×25 Å cubic cell with the N*V*T ensemble. For the bulk system, simulations (Fig. 5) are conducted at 500 K using the unit cell with single k point in the N*p*T ensemble (varying shape and volume). The pair correlation functions are calculated using atomic trajectory data collected for 100 ps after 20 ps was allowed to reach thermal equilibrium.

Acknowledgements

This work is supported in part by the U. S. Department of Energy, Office of Basic Energy Sciences, Division of Materials Sciences and Engineering under Award # DE-FG02-96ER45579. We acknowledge resources of the National Energy Research Scientific Computing Center supported by the Office of Science of the U.S. Department of Energy under Contract No. DE-AC02-05CH11231.

Supporting Information

Two special solutions of Eq. (1) and (2) in the paper; Figure S1: optimized ground states of pseudohalides in Table 1; Figure S2: optimized crystal structures of $MAPbI_{2.75}(OCl)_{0.25}$ and $MAPbI_{2.75}(OBr)_{0.25}$, together with their calculated band structures with (in red) and without (in black) the spin-orbit coupling (SOC); Figure S3: optimized cluster models of $MAPbI_2(OCl)$ and $MAPbI_2(OBr)$; Figure S4: optimized water-cluster complexes of $MAPbI_2(SCN)•H_2O$ and $MAPbI_2(SeCN)•H_2O$; Figure S5: optimized crystal structures of $MAPbI_3$, $MAPbI_{2.75}(S/SeCN)_{0.25}$, $MAPbI_{2.75}(PCO)_{0.25}$ and $MAPbI_{2.75}(OI)_{0.25}$ with the insertion of one water molecule; Figure S6: key steps showing the phase transition of $MAPbI_{2.75}(PCO)_{0.25}$ caused by water and the formation of the "CH_3NH_2 + O-H" defect inside $MAPbI_{2.75}(OI)_{0.25}•H_2O$; Figure S7: initial structure of $MAPbI_{2.75}(OI)_{0.25}$ with the "CH_3NH_2 + O-H" defect without and with the rotation of CH_3NH_2.

References

(1) Mitzi, D. B., Field, C. A., Harrison, W. T. A. and Guloy, A. M. Conducting tin halides with a layered organic-based perovskite structure. *Nature*, **1994**, *369*, 467.

(2) Lee, M. M., Teuscher, J., Miyasaka, T., Murakami, T. N. and Snaith, H. J. Efficient hybrid solar cells based on meso-superstructured organometal halide perovskites. *Science*, **2012**, *338*, 643.

(3) Etgar, L., Gao, P., Xue, Z., Peng, Q., Chandiran, A. K., Liu, B., Nazeeruddin, M. K. and Graetzel, M. Mesoscopic $CH_3NH_3PbI_3/TiO_2$ heterojunction solar cells. *J. Am. Chem. Soc.*, **2012**, *134*, 17396.

(4) Hodes, G. Perovskite-based solar cells. *Science*, **2013**, *342*, 317.

(5) Loi, M. A. and Hummelen, J. C. Hybrid solar cells: perovskites under the sun. *Nature Mat*., **2013**, *12*, 1087.

(6) Noh, J. H., Im, S. H., Heo, J. H., Mandal, T. N. and Seok, S. I. Chemical management for colourful, efficient, and stable inorganic-organic hybrid nanostructured solar cells. *Nano Lett*., **2013**, *13*, 1764 (2013).

(7) Snaith, J. H. Perovskites: the emergence of a new era for low-cost, high-efficiency solar cells. *J. Phys. Chem. Lett*., **2013**, *4*, 3623.

(8) Park, N. G. Organometal perovskite light absorbers toward a 20% efficiency low-cost solid-state mesoscopic solar cell. *J. Phys. Chem. Lett*., **2013**, *4*, 2423.

(9) Bisquert, J. The swift surge of perovskite photovoltaics. *J. Phys. Chem. Lett*., **2013**, *4*, 2597.

(10) Lotsch, B. V. New light on an old story: perovskites go solar. *Angewandte Chemie International Edition*, **2014**, *53*, 635.

(11) Hao, F., Stoumpos, C. C., Cao, D. H., Chang, R. P. H. and Kanatzidis, M. G. Lead-free solid-state organic-inorganic halide perovskite solar cells. *Nature Photonics*, **2014**, *8*, 489.

(12) Misra, R. K., Aharon, S., Li, B., Mogilyansky, D., Visoly-Fisher, I., Etgar, L. and Katz, E. A. Temperature- and component-dependent degradation of perovskite photovoltaic materials under concentrated sunlight. *J. Phys. Chem. Lett*., **2015**, *6*, 326.

(13) Deretzis, I., Alberti, A., Pellegrino, G., Smecca, E., Giannazzo, F., Sakai, N., Miyasaka, T. and La Magna, A. Atomistic origins of $CH_3NH_3PbI_3$ degradation to PbI_2 in vacuum. *Appl. Phys. Lett*., **2015**, *106*, 131904.

(14) Frost, J. M., Butler, K. T., Brivio, F., Hendon, C. H., van Schilfgaarde, M. and Walsh, A. Atomistic origins of high-performance in hybrid halide perovskite solar cells. *Nano Lett*., **2014**, *14*, 2584.

(15) Fang, H.; Jena, P. Super-ion inspired colorful hybrid perovskite solar cells. *J. Mater. Chem. A*, **2016**, *4*, 4728-4737.

(16) Yang, S., Wang, Y., Liu P., Cheng Y., Zhao, H. and Yang, H. Functionalization of perovskite thin films with moisture-tolerant molecules. *Nat. Energy*, **2016**, *1*, 15016.

(17) Habisreutinger, S., McMeekin, D., Snaith, H. and Nicholas, R. Reserach update: strategies for improving the stability of perovskite solar cells. *APL Mater*., **2016**, *4*, 091503.

(18) Eperon, G., Leijtens, T., Bush, K., Prasanna, R., Green, T., Wang, J. T.-W., McMeekin, D., Volonakis, G., Milot, R., May, R. *et al*., Perovskite-perovskite tandem photovoltaics with optimized bandgaps. *Science*, **2016**, 10.1126/science.aaf9717.

(19) Tai, Q., You, P., Sang, H., Liu, Z., Hu, C., Chan, H. and Yan, F. Efficient and stable perovskite solar cells prepared in ambient air irrespective of the humidity. *Nat. Commun*. **2016**, *7*, 11105.

(20) Fang, H. and Jena, P. Molecular origin of properties of organic–inorganic hybrid perovskites: the big picture from small clusters. *J. Phys. Chem. Lett*., **2016**, *7*, 1596-1603.

(21) Yao, Q., Fang, H., Deng, K., Kan, E. and Jena, P. Super-halogens as building blocks of two-dimensional organic-inorganic hybrid perovskites for optoelectronics applications. *Nanoscale*, **2016**, *8*, 17836-17842.

(22) Gutsev, G. L. and Boldyrev, A. I. DVM Xα calculations on the electronic structure of "superalkali" cations. *Chem. Phys. Lett.*, **1982**, *92*, 262.

(23) Gutsev, G. L. and Boldyrev, A. I. DVM-Xα Calculations on the ionization potentials of MX_{k+1}^- complex anions and the electron affinities of MX_{k+1} "superhalogens". *Chem. Phys. Lett*., **1981**, *56*, 277-283.

(24) Fang, H. and Jena, P. $B_{12}(SCN)_{12}^-$: An ultrastable weakly coordinating dianion. *J. Phys. Chem*. C, **2017**, *121*, 7697–7702.

(25) Filip, M. R., verdi, C. and Giustino, F. GW band structures and carrier effective masses of $CH_3NH_3PbI_3$ and hypothetical perovskites of the type $APbI_3$: A = NH_4, PH_4, AsH_4, and SbH_4. *J. Phys. Chem. C*, **2015**, *119*, 25209-25219.

(26) Miyata, A.; Mitioglu, A.; Plochocka, P.; Potrugall, O.; Wang, J. T.-W.; Stranks, S. D.; Snaith, H. J.; Nicholas, R. J. Direct measurement of the exciton binding energy and effective masses for charge carriers in an organic-inorganic tri-halide perovskite. *Nat. Phys*., **2015**, *11*, 582-587.

(27) Zheng, F., Tan, L., Liu, S. and Rappe, A. Rashba spin-orbit coupling enhanced carrier lifetime in $CH_3NH_3PbI_3$. *Nano Lett*., **2015**, *15*, 7794-7800.

(28) Niesner, D., Wilhelm, M., Levchuk, I., Osvet, A., Shrestha, S., Batentschuk, M., Brabec, C. and Fauster, T. Giant Rashba splitting in $CH_3NH_3PbBr_3$ organic-inorganic perovskite. *Phys. Rev. Lett*., **2016**, *117*, 126401.

(29) Etienne, T. Mosconi, E. and Angelis, F. dynamical origin of the Rashba effect in organohalide lead perovskites: a key to supperssed carrier recombination in perovkite solar cells? *J. Phys. Chem. Lett*., **2016**, *7*, 1638-1645.

(30) Frisch, M. J. Gaussian03, revision B. 03; Gaussian, Inc.: Wallingford, CT, **2003**.

(31) Becke, A. Density-functional thermochemistry. III. the role of exact exchange. *J. Chem. Phys*., **1993**, *98*, 5648-5652.

(32) Lee, C.; Yang, W.; Parr, R. G. Development of the Colle-Salvetti correlation-energy formula into a functional of the electron density. *Phys. Rev. B*, **1988**, *37*, 785-788.

(33) Pewdew, J. P., Burke, K., Ernzerhof, M. Generalized gradient approximation made simple. *Phys. Rev. Lett*., **1996**, *77*, 3865.

(34) Kresse, G. and Furthmueller, J. Efficiency of ab-initio total energy calculations for metals and semiconductors using a plane-wave basis set. *J. Comput. Mater. Sci*., **1996**, *6*, 15-50.

(35) Kresse, G. and Furthmueller, J. Efficient iterative schemes for ab initio total-energy calculations using a plane-wave basis set. *Phys. Rev. B*, **1996**, *54*, 11169-11186.

(36) Fang, H., Gu, M., Liu, B., Liu, X., Huang, S., Ni, C., Li, Z. and Wang, R. Plane-wave pseudopotential study for the structural stability of Hf: the role of spin-orbit interaction. *Physica B*, **2011**, *406*, 1744-1748.

(37) Grimme, S. Semiempirical GGA-type density functional constructed with a long-range dispersion correction. *J. Comput. Chem*., **2006**, *27*, 1787.

(38) Fang, H., Dove, M. and Refson, K. Ag-Ag dispersive interaction and physical properties of $Ag_3Co(CN)_6$. *Phys. Rev. B*, **2014**, *90*, 054302.